Available online at www.sciencedirect.com
ScienceDirect
Thin Solid Films 516 (2008) 2874–2880
www.elsevier.com/locate/tsf

Deposition and dielectric properties of $CaCu_3Ti_4O_{12}$ thin films deposited on $Pt/Ti/SiO_2/Si$ substrates using radio frequency magnetron sputtering

B. Shri Prakash [a], K.B.R. Varma [a,*], Dominique Michau [b], Mario Maglione [b]

[a] *Materials Research Centre, Indian Institute of Science, Bangalore, 560012, India*
[b] *Ferroelectric Materials Division, ICMCB-CNRS, ICMCB-Institute of Condensed Matter Chemistry of Bordeaux, 33608 Pessac Cedex, France*

Received 14 August 2006; received in revised form 1 May 2007; accepted 24 May 2007
Available online 6 June 2007

Abstract

Polycrystalline $CaCu_3Ti_4O_{12}$ thin films were deposited on $Pt(111)/Ti/SiO_2/Si$ substrates using radio frequency magnetron sputtering. The phase formation and the physical quality of the films were crucially dependent on the substrate temperature and oxygen partial pressure. Good quality films were obtained at a substrate temperature of 650 °C and 4.86 Pa total pressure with 1% O_2. The dielectric constant (~5000 at 1 kHz and 400 K) of these films was comparable to those obtained by the other techniques, eventhough, it was much lower than that of the parent polycrystalline ceramics. For a given temperature of measurements, dielectric relaxation frequency in thin film was found to be much lower than that observed in the bulk. Also, activation energy associated with the dielectric relaxation for the thin film (0.5 eV) was found to be much higher than that observed in the bulk ceramic (0.1 eV). Maxwell–Wagner relaxation model was used to explain the dielectric phenomena observed in $CaCu_3Ti_4O_{12}$ thin films and bulk ceramics.

Keywords: Ceramics; Dielectric properties; Sintering; X-ray diffraction

1. Introduction

High dielectric constant oxide materials are of much interest because of their importance in the miniaturization of electronic devices [1–3]. This has led to a quest among the scientific community to improve upon the dielectric properties of the existing ferroelectric/relaxor materials such as barium titanate [4,5], lead zirconate titanate [6] or barium strontium titanate [3,7]. However, the dielectric properties of these materials are strongly temperature dependent and undergo a maximum in the vicinity of the ferroelectric to paraelectric transition temperatures. These characteristics are undesirable from the electronic device applications view point. In this context, the discovery of $CaCu_3Ti_4O_{12}$ (CCTO) has generated an immense interest owing to its giant dielectric constant despite its centrosymmetric nature (space group Im3) [8–11].The polycrystalline CCTO was reported to exhibit remarkably high dielectric constant $>10^4$ [8,9,11,12] at 100 kHz at 300 K. However, these properties were strongly dependent on processing conditions [13–17]. The value of dielectric constant for a single crystal of CCTO was reported to be close to 10^5 [10]. Further, the dielectric constant was reported to remain constant in the 100–400 K temperature range. When the temperature was lowered below 100 K the dielectric constant decreased by three orders of magnitude. The dielectric constant value was as low as 100 below 100 K [8–10]. However, neither a phase transition nor a detectable long-range crystal structural change was found by high resolution X-ray and neutron diffraction studies in the temperature range of 100–600 K [8,9]. In the frequency domain, it showed an extremely high value of dielectric constant (up to 10^5) at room temperature (300 K) in the 100 Hz–1 MHz frequency range and exhibited a dielectric relaxation above this frequency. The value of dielectric constant above the relaxation frequency was as low as 80 and frequency of dielectric relaxation was dependent on the measurement temperature [8–10]. Such a high dielectric constant is usually a characteristic feature of ferroelectric materials with the permanent dipoles being the major contributors for the

* Corresponding author. Tel.: +91 80 2293 2914; fax: +91 80 2360 0683.
E-mail address: kbrvarma@mrc.iisc.ernet.in (K.B.R. Varma).

0040-6090/$ - see front matter © 2007 Elsevier B.V. All rights reserved.
doi:10.1016/j.tsf.2007.05.060

polarization. But, the origin of high dielectric constant in CCTO due to the permanent dipoles is ruled out because of its centrosymmetric nature (Im3) even down to 35 K [18].

The origin of the giant dielectric constant in CCTO is not well understood yet. However, the recent papers based on the impedance spectroscopy revealed its extrinsic nature owing to the huge difference that exists in the resistivity of grain and the grain boundary leading to the barrier layer capacitor-like situation [12,13]. Further, the studies concerning the electrode material and thickness effects demonstrated their strong influence on the dielectric properties of CCTO ceramics. Since, it is practically difficult to scale down the thickness beyond a certain level without being supported by some substrate, we thought it was worth fabricating thin films of CCTO on industrially important substrates such as Pt(111)/Si(100). There have been a few reports on CCTO thin films deposited by pulsed laser depositions (PLD) and chemical solution route [19–22]. However, there are no reports on the CCTO films deposited by sputtering technique. In this paper we report the details pertaining to the deposition and dielectric properties of CCTO thin films on Pt(111)–Si(100) substrates by radio frequency (RF) magnetron sputtering.

2. Experimental details

Polycrystalline ceramic powders of CCTO was prepared via the conventional solid-state reaction route using stoichiometric amounts of $CaCO_3$, CuO, and TiO_2. These were thoroughly mixed in an acetone medium using a ball mill. Subsequently the mixture was oven dried for about 2 h. This was followed by the calcination of the powder at 1000 °C for 10 h with an intermittent grinding. The formation of the monophasic compound was confirmed by X-ray powder diffraction (XRD) using monochromatic Cu K_α ($\lambda = 1.541$ Å) radiation. The polycrystalline powder was then cold pressed into a disk of 5 cm in diameter and 4 mm in thickness at a pressure of 30 MPa using PVA as binder. The pressed target was slowly heated to 600 °C to get rid of the binder and finally sintered in air at 1050 °C for 10 h.

Pt(111)/Ti/SiO_2/Si(100) substrate was used for deposition of the films. The target to substrate distance was 5 cm. Prior to the deposition, sputtering chamber was evacuated to 333.3×10^{-7} mPa using rotary and turbomolecular pumps. The deposition was carried out using a mixture of argon (Ar) and oxygen (O_2) with different amounts of O_2 and at two different total pressures of 4.86 Pa and 5.9 Pa. For each total pressure, the Ar/O_2 flow rates set were 99/1, 95/5 and 90/10 sccm. This corresponds to O_2 partial pressures of 48.66 mPa, 243.3 mPa and 486 mPa respectively for the total pressure of 4.86 Pa. The deposition was carried out at 50 W (3.5 W/cm^2) power. Substrate temperatures were varied from room temperature to 800 °C. Deposition duration was varied from 1 h to 8 h to calculate the deposition rate. The resulting film thicknesses were determined by surface profilometry, and ranged from 50 nm to 400 nm corresponding to the deposition rate of 50 nm/h for the film deposited at 650 °C, total pressure of 4.86 Pa and O_2/Ar ratio of 5/95 sccm. The formation of the monophasic film was confirmed via XRD using monochromatic Cu K_α radiation. The composition of the film was analyzed by Electron probe microanalysis (EPMA) and Rutherford backscattering (RBS) experiments. For carrying out the electrical measurements, samples in the form of metal-insulator-metal sandwich structure were fabricated. For this, Pt dots of 150 μm diameter were deposited on to the CCTO films at room temperature through a shadow mask by RF sputtering technique. The capacitance measurements were carried out as a function of frequency (100 Hz–15 MHz) and temperature (100–450 K) using impedance gain phase analyzer (HP4194A) at a signal strength of 0.1 V_{rms}. For comparison, capacitance measurements were also performed on polycrystalline ceramic pellets sintered at 1100 °C for 10 h.

3. Results and discussion

Fig. 1(a and b) shows the XRD patterns obtained for the CCTO films (Fig. 1a) grown on Pt(111)–Si(100) at a total pressure of 36.5 mT with 1% O_2 and at a substrate temperature of 650 °C and CCTO bulk ceramic target (Fig. 1b). The XRD pattern obtained for the film in the angle range 45°–65° has been shown separately in the inset of Fig. 1a to highlight the low intensity peaks in this range. The XRD pattern of the film show distinct (2 2 0), (4 4 0) and (4 2 2) peaks along with other low intensity peaks, which matches well with the corresponding peaks in the polycrystalline bulk ceramic of CCTO, demonstrating its polycrystalline characteristics. However, compared with the bulk ceramics, intensities of (2 2 0) and (4 4 0) peaks in

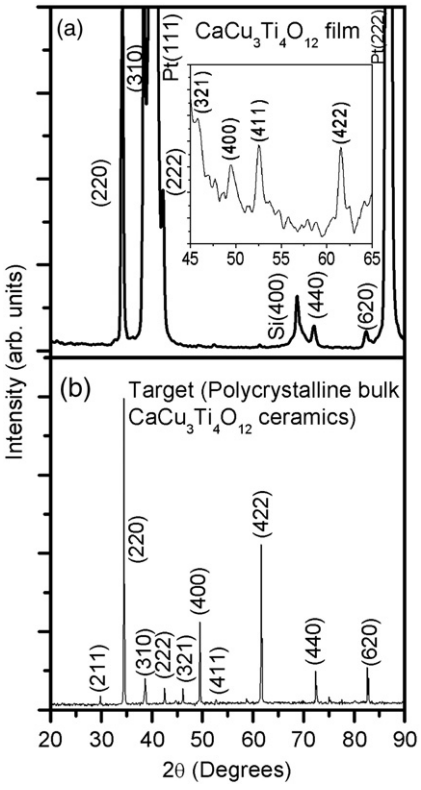

Fig. 1. XRD patterns for (a) polycrystalline $CaCu_3Ti_4O_{12}$ ceramic target sintered at 1050 °C/10 h (b) $CaCu_3Ti_4O_{12}$ films grown on Pt(111)–Si(100) substrate at a total pressure of 4.86 Pa with 1% O_2 and at a substrate temperature of 650 °C.

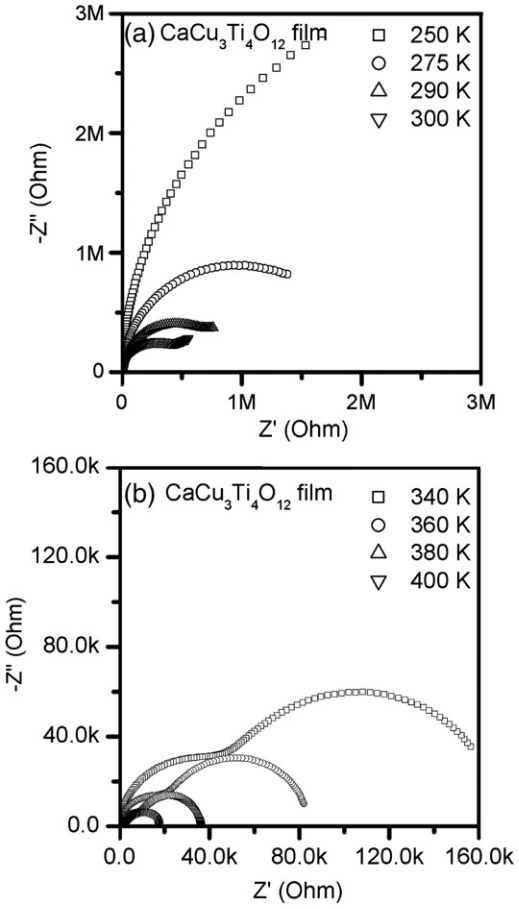

Fig. 2. Complex impedance plots for the $CaCu_3Ti_4O_{12}$ film at two different temperature ranges (a) 250–300 K (b) 340–400 K.

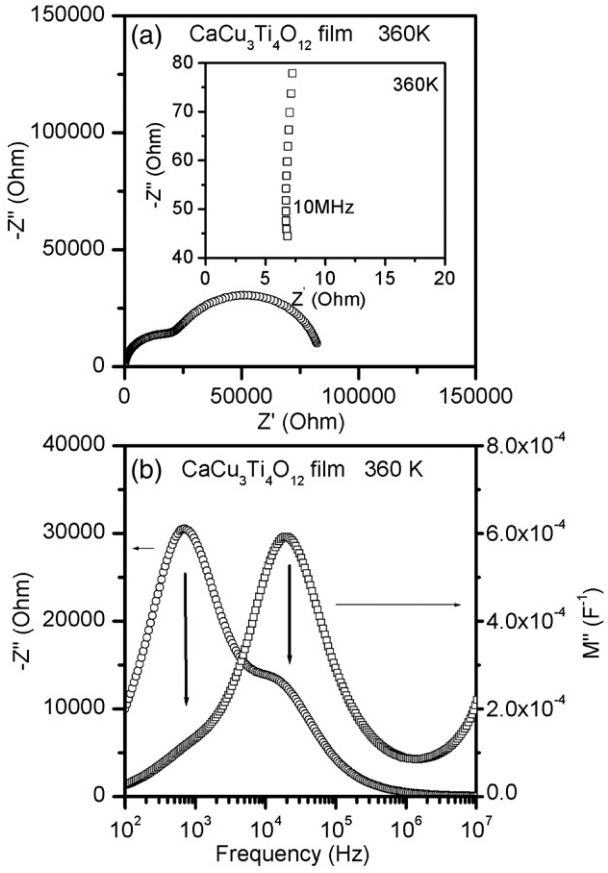

Fig. 3. (a) Complex impedance plot at 360 K for the $CaCu_3Ti_4O_{12}$ film. The inset in (a) shows the expanded view of the high frequency impedance data for the $CaCu_3Ti_4O_{12}$ film at 360 K (b) Combined (Z'', M'') spectroscopic plot for the $CaCu_3Ti_4O_{12}$ film at 360 K.

the film are much higher than the rest of the peaks from planes, indicating the preferential (2 2 0) orientation in the film. This pattern confirms the polycrystalline nature of the as-grown film with preferential (2 2 0) orientation. The analyses by EPMA and RBS confirmed that the composition of the film to be that of CCTO. Good quality continuous films were obtained on adopting the above deposition parameters. On increasing the substrate temperature to 850 °C, additional phases apart from CCTO started appearing as confirmed by XRD studies. An increase, either in total pressure or O_2 partial pressure led to the breakage of the film which would not qualify for dielectric studies. The films of ~250 nm in thickness were chosen for electrical measurements that are reported in this paper.

Fig. 2(a and b) shows the impedance plots (Z^* plots) at different temperatures for the as deposited film. $-Z''$ vs Z' plots at 250 K and below exhibit only an arc due to the high impedance associated with the film. There exists one semicircle with a tail at the low frequency end above 250 K. The Z^* plots at 300 K and above exhibit two overlapping semicircles with a nonzero intercept on the Z' axis at high frequency end (inset of Fig. 3a). Fig. 3 shows the Z^* plots at 360 K (Fig. 3a) along with the combined $-Z''$, M'' vs f (frequency) plot (Fig. 3b). The combined $-Z''$, M'' plots clearly demonstrate the presence of two Debye-like peaks in each spectrum. The presence of small high frequency nonzero intercept on Z' axis in the Z^* plot (inset of Fig. 3a) and the presence of high frequency incline in the M'' spectrum (Fig. 3b) suggest the existence of the semiconductive and low capacitive regions. Based on these observations, the Z^* data above 340 K were analyzed using the equivalent circuit consisting of a resistor connected in series with two resistor–capacitor (RC) elements as shown in the Fig. 4, element R_g representing the grain, $R_{gb}C_{gb}$ representing the grain boundary and $R_{el}C_{el}$ representing the electrode–sample interface. Where R_g is the grain resistance. R_{gb}, R_{el} and C_{gb}, C_{el} are the resistance and capacitance associated with the grain boundary and the

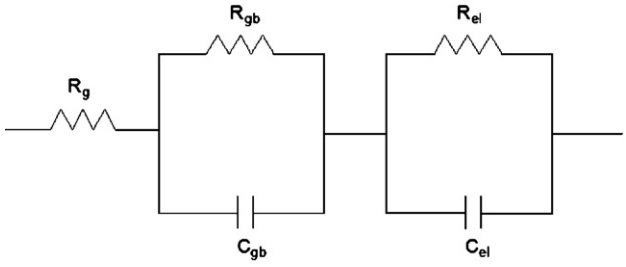

Fig. 4. Equivalent circuit model to describe the electrical properties of $CaCu_3Ti_4O_{12}$ film.

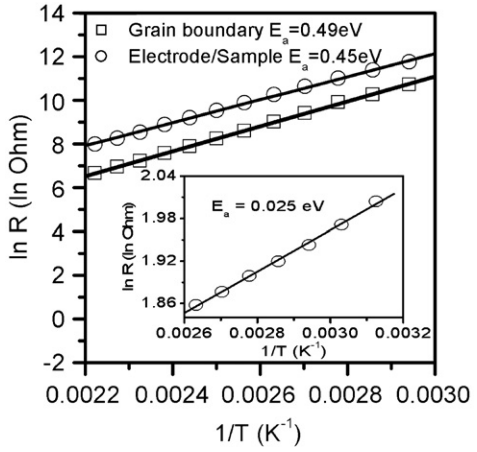

Fig. 5. Arhenius plots for resistance of grain boundary and electrode–sample interface for $CaCu_3Ti_4O_{12}$ films. Inset in the figure is the Arhenius plot for grain region in the film.

electrode–sample interface respectively. Each semicircle in the Z^* plot (Fig. 3a) is described well by Cole–Cole equation.

$$Z^* = \frac{R}{1 + (i\omega\tau)^{\alpha}} \tag{1}$$

Where $\tau = RC$ and the parameter α, $0 < \alpha \leq 1$, is used to measure the departure from ideal Debye response. The fitted value of α at different temperatures for both semicircles are in the range of 0.93–0.97, reflecting the nearly Debye nature of these regions in the sample. Based on the equivalent circuit that is depicted in Fig. 4, and in accordance with the brickwork layer model for electroceramics, the large semicircle observed at lower frequency region with $R \sim 65$ kΩ and $C \sim 6.3$ nF was attributed to the electrode–sample interface response, the semicircle in the high frequency range with $R \sim 20$ kΩ and $C \sim 0.58$ nF was attributed to grain boundary response and the nonzero intercept on the Z'-axis at high frequency end was attributed to the bulk resistance, R_g.

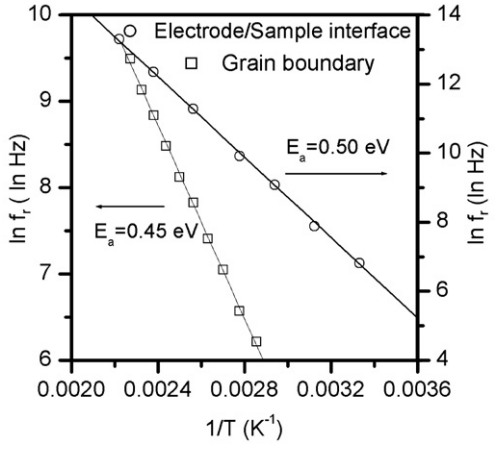

Fig. 6. Arhenius plots for relaxation frequencies calculated from combined (Z'', M'') spectroscopic plots corresponding to the electrode–sample interface and the grain boundary for $CaCu_3Ti_4O_{12}$ films.

In the combined $-Z''$, M'' plot (Fig. 3b), Z'' plot is dominated by the most resistive element, i.e., electrode–sample interface, R_{el}, where as M'' plot is dominated by the element with relatively smaller capacitance i.e. grain boundary. In Z'' plot, the peak corresponding to grain boundary appears only as a shoulder due to its low resistance as compared to the electrode–sample interface. In the M'' plot, the response from electrode–sample interface appears only as a small hump owing to the high capacitance associated with it. As shown in Fig. 2b, resistances corresponding to each region decreases with increase in the temperature and are plotted against the reciprocal of temperature in the Arhenius format (Fig. 5). All the three regions obeyed Arhenius law with activation energies of 0.45 eV (electrode), 0.49 eV (grain boundary) and 0.025 eV (grain) (Fig. 5). Relaxation frequencies corresponding to electrode–sample interface and the grain boundary also followed the Arhenius law with activation energies of 0.45 eV and 0.50 eV (Fig. 6), which are nearly equal to the activation energies obtained from resistance values for these two regions (0.45 eV and 0.49 eV respectively) (Fig. 5). Two nearly equal activation energies obtained for conduction and relaxation reveal that the resistance and relaxation time ($\tau = 1/f_r$) decrease at a similar rate with increase in temperature.

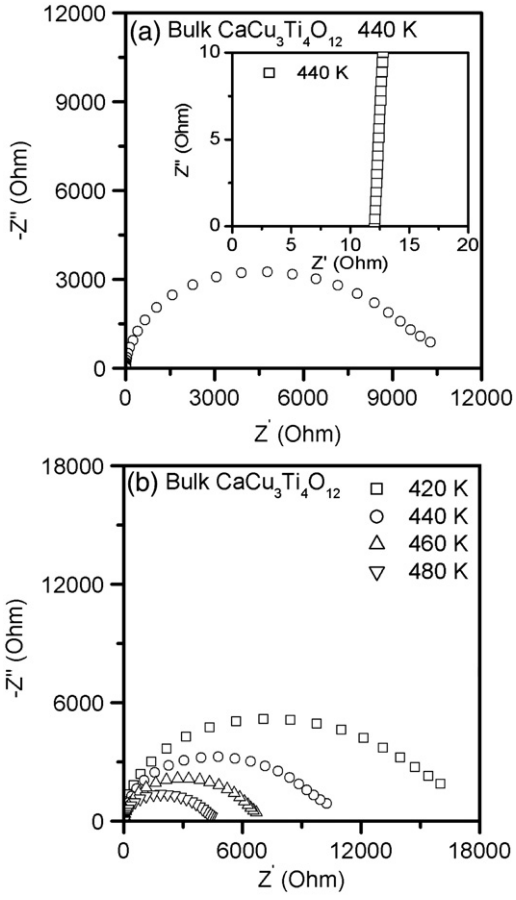

Fig. 7. (a) Complex impedance plots for the $CaCu_3Ti_4O_{12}$ ceramics at 440 K, (b) complex impedance plots of $CaCu_3Ti_4O_{12}$ ceramics at different temperatures. Inset of (a) shows the expanded view of the high frequency impedance data for the $CaCu_3Ti_4O_{12}$ bulk ceramics at 440 K.

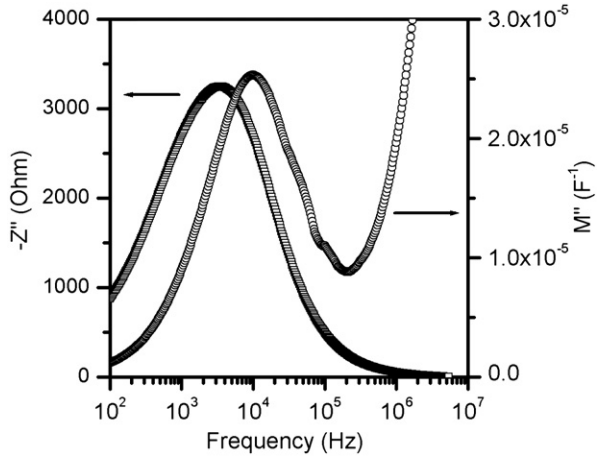

Fig. 8. Combined (Z'', M'') spectroscopic plot for the $CaCu_3Ti_4O_{12}$ bulk ceramics.

For comparison, impedance plots of the polycrystalline ceramic pellet sintered at 1100 °C for 10 h at different temperatures are shown in Fig. 7(a–b). It exhibits only one semicircle with nonzero intercept on Z'-axis at higher frequency. The semicircle is ascribed to originate from the grain boundary and nonzero intercept corresponding to the resistance of the grain, with no semicircle corresponding to electrode–sample interface. The combined $-Z''$, M'' spectroscopic plot also shows the presence of only one Debye-like peak in each spectrum (Fig. 8). The presence of both high frequency nonzero intercept on Z'-axis in the Z^* plot (inset of Fig. 7a) and high frequency incline in the M'' spectrum at $f > 10^6$ Hz (Fig. 8) indicate the existence of semiconductive and low capacitive regions in the sample. Based on the equivalent circuit that is depicted in Fig. 4, and in accordance with the brickwork layer model for electroceramics, the large semicircle observed at lower frequency region was attributed to grain boundary and the nonzero intercept on the Z'-axis at high frequency end was attributed to the grain resistance. The activation energies corresponding to grain and the grain boundary are calculated from the variation of grain and the grain boundary resistances with temperature and these are 0.07 eV and 0.73 eV respectively (Fig. 9).

It could be noted that the activation energies obtained for grain and the grain boundary conduction in thin films is much lower than that found in bulk ceramic. Thin films with their much reduced size in one dimension are expected to have higher defect density than that in the corresponding polycrystalline bulk ceramics even on annealing them in the oxygen atmosphere at elevated temperatures, which might result in the lower activation energy for conduction in case of thin film. The other possible reason for the low value of the activation energy could be due to the strain associated with the film owing to the lattice mismatch between the film and the substrate. In addition, vast difference in the microstructural features between the bulk and the film could also lead to above differences in the activation energy value. Bulk ceramics that was used for the impedance measurement consisted of grains with an average size of 40–50 μm. On the other hand, films had very small grains resulting in the higher density of the grain boundary and so will be the number of the defects. All these factors might enable oxygen ions to migrate

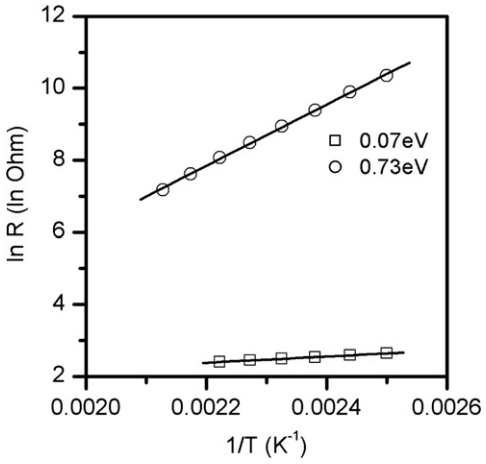

Fig. 9. Arhenius plots of grain and the grain boundary resistance for $CaCu_3Ti_4O_{12}$ bulk ceramics.

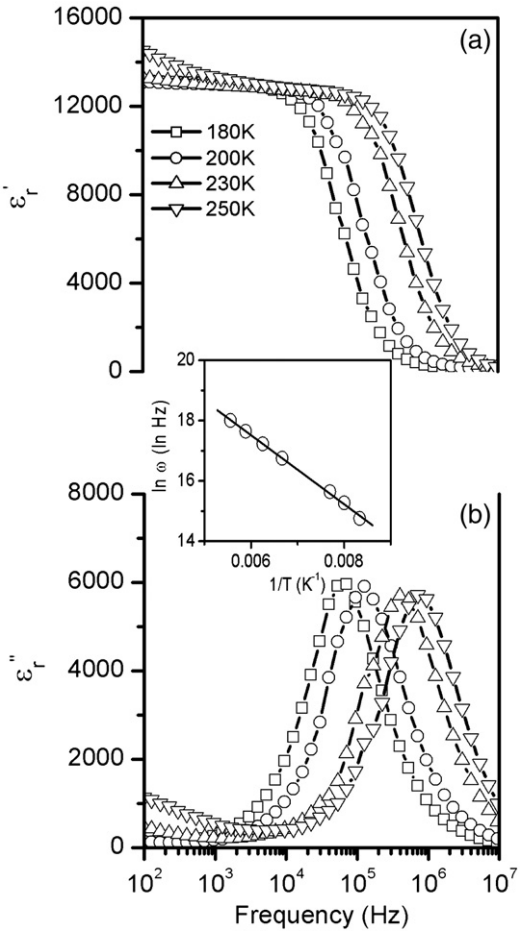

Fig. 10. Variation in the real (ε'_r) and imaginary parts (ε''_r) of the dielectric constant with frequency for polycrystalline $CaCu_3Ti_4O_{12}$ bulk ceramics at different temperatures. Inset shows Arhenius plot for frequency of dielectric relaxation.

with lower activation energy at the grain boundary in the case of thin films. Same argument can also explain the lower activation energy obtained for grain conduction in thin films when compared to bulk ceramics as the density of the polarons depends on the density of defects in the film.

The variation in the real (ε_r') and imaginary parts (ε_r'') of the dielectric constant with frequency for polycrystalline bulk ceramic at different temperatures is shown in Fig. 10. ε_r' decreases from a constant value at low frequency to a small saturated value at high frequency. The values of the dielectric constant in lower and higher plateau regions are nearly 13,000 and 100 respectively. Correspondingly, ε_r'' clearly shows a Debye-like relaxation peak shifting to higher frequencies with increasing temperatures. The relaxation frequency (f_r) followed an Arhenius law with activation energy of 0.1 eV, which is close to the activation energy for the grain conduction process (0.07 eV).

The variation in the ε_r' and ε_r'' with frequency for the present polycrystalline film at different temperatures is shown in Fig. 11 (a and b). The dielectric behavior of the film is similar to that of the bulk ceramic with the dielectric constant decreasing from a constant value (~5000) at low frequency to a small saturated value at high frequency. The observed dielectric constant at low frequency is much smaller than that reported for bulk ceramics.

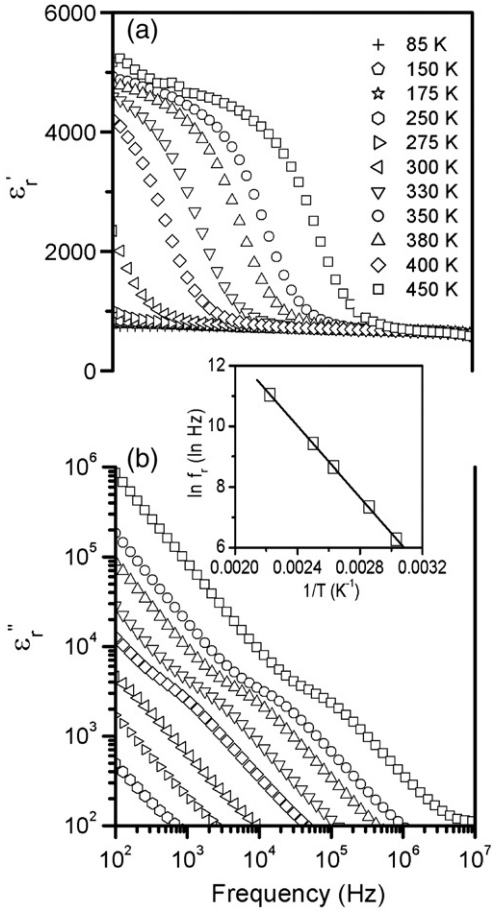

Fig. 11. Variation in the real (ε_r') and imaginary parts (ε_r'') of the dielectric constant with frequency for polycrystalline $CaCu_3Ti_4O_{12}$ films at different temperatures.

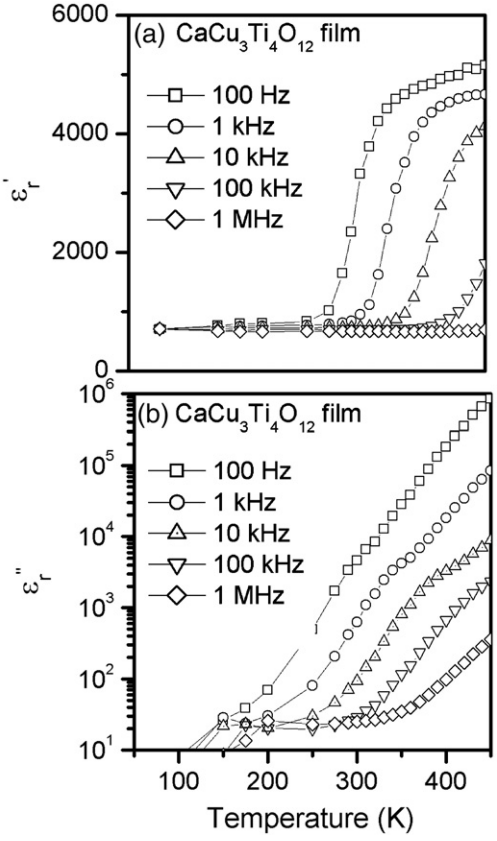

Fig. 12. Variation in the real (ε_r') and imaginary parts (ε_r'') of the dielectric constant with temperature for polycrystalline $CaCu_3Ti_4O_{12}$ films at representative frequencies.

However, the value is comparable with that reported for CCTO thin films deposited by other techniques such as PLD [20–22] and chemical method [23]. The only difference that is observed in the present case is the frequency at which the drastic reduction in dielectric constant occurred. The frequency of dielectric relaxation is much lower in the case of film than that of the bulk ceramic. However, the Debye-type relaxation is hardly realized in the loss peak. Because of high conductivity in the low frequency regime, which is linear on a log–log scale, the loss peak appears only as a shoulder. Nevertheless, this peak follows the real part relaxation frequency, which increases as the temperature increases. The relaxation frequency is found to follow Arhenius law with activation energy of 0.5 eV, which is equal to the activation energy corresponding to the grain boundary conduction (Inset of Fig. 11). Fig. 12 shows the variation in the ε_r' and ε_r'' with temperature for polycrystalline CCTO films at representative frequencies. Eventhough the variation is similar to the one that exhibited by the bulk polycrystalline CCTO ceramic, the temperature at which the step increase in the ε_r' occurs in the film is much higher than that in the case of the bulk ceramics..

The large dielectric constant associated with CCTO bulk ceramics has been explained based on the Maxwell–Wagner phenomenon at the grain boundary, which gives rise to a relaxation spectrum similar to the Debye relaxation. The characteristic frequency (f_r) of such dielectric relaxation is decided by the

resistance and capacitance of grain and the grain boundary according to the following equation [24],

$$f_r = \frac{1}{2\pi}\left[\frac{R_g + R_{gb}}{R_g R_{gb}(C_g + C_{gb})}\right]$$

In CCTO ceramic, $R_{gb} \gg R_g$ and $C_{gb} \approx 10C_g$, hence, relaxation frequency becomes approximately equals to

$$f_r \approx \frac{1}{2\pi}\left[\frac{1}{R_g C_{gb}}\right]$$

The above equation for f_r clearly explains near equivalent values for the activation energies obtained for grain conduction (0.07 eV) and dielectric relaxation (0.1 eV), provided C_{gb} has rather weak temperature dependence, which is very much true in CCTO ceramics. Hence, the near equivalence of activation energy values for dielectric relaxation (0.5 eV) in thin film and for its grain boundary conduction (0.49 eV) and weak temperature dependence of C_{el} suggests that the observed dielectric phenomenon in thin films may be originating from electrode–sample interface, wherein dielectric relaxation frequency is given by,

$$f_r \approx \frac{1}{2\pi}\left[\frac{1}{R_{gb} C_{el}}\right]$$

As explained above, root cause for the dielectric relaxation in bulk CCTO ceramic and thin film seems to be totally different. In CCTO bulk ceramic, the dielectric relaxation is reported to be from grain boundary to the grain [12]. On the other hand, in case of thin film, it is appears to be from electrode–sample interface to the grain boundary. The support for this presumption can also be obtained from ε_r' vs f graphs for bulk (Fig. 10) and thin film (Fig. 11) on close observation. It is clear from these graphs that for a given temperature, the frequency of dielectric relaxation in case of film is much lower than that of the bulk ceramic. Above arguments clearly suggest that the reason for the dielectric relaxation bulk and thin film are different and hence their activation energies.

4. Conclusions

Polycrystalline $CaCu_3Ti_4O_{12}$ thin films were deposited on Pt (111)/Ti/SiO_2/Si substrates using RF-magnetron sputtering. The substrate temperature, total chamber pressure and oxygen partial pressure had great influence on physical quality and the phase formation of the films. Good quality films were obtained at a substrate temperature of 650 °C and 4.86 Pa total pressure with 1% O_2 were. The XRD studies revealed the polycrystalline nature of the film with preferential (2 2 0) orientation. The 250 nm film had a fairly high dielectric constant of dielectric constant of 5000 at 1 kHz and 400 K, which is comparable to that obtained for the films deposited by the other techniques such as pulsed laser deposition and chemical methods. However, the value was much lower than that obtained for the polycrystalline bulk ceramics. Frequency of dielectric relaxation in thin films was found to be much lower that observed in the bulk ceramic for a given temperature of measurement. In addition, activation energy associated with the dielectric relaxation in thin film was found to be much higher than that observed in the bulk ceramics. Based on the Maxwell–Wagner relaxation model, the dielectric relaxation observed in thin film was attributed to be originating from electrode–sample interface and the one that is found in bulk ceramic was ascribed to be from grain boundary.

Acknowledgements

The authors thank the Department of Science and Technology (DST), Government of India for financial grant. One of the authors (B. Shri Prakash) thanks the French Embassy, New Delhi, for sponsoring his visit through LAFICS to ICMCB, Bordeaux, France.

References

[1] P.C. Joshi, M.W. Cole, Appl. Phys. Lett. 77 (2000) 289.
[2] W.J. Kim, W. Chang, S.B. Qadri, J.M. Pond, S.W. Kirchoefer, D.B. Chrisey, J.S. Horwitz, Appl. Phys. Lett. 76 (2000) 1185.
[3] W. Chang, J.S. Horwitz, A.C. Carter, J.M. Pond, S.W. Kirchoefer, C.M. Gilmore, D.B. Chrisey, Appl. Phys. Lett. 74 (1999) 1033.
[4] S.M. Bobade, D.D. Gulwade, A.R. Kulkarni, P. Gopalan, J. Appl. Phys. 97 (2005) 074105.
[5] M.T. Buscaglia, M. Viviani, V. Buscaglia, L. Mitoseriu, A. Testino, P. Nanni, Z. Zhao, M. Nygren, C. Harnagea, D. Piazza, C. Galassi, Phys. Rev., B 73 (2006) 64114.
[6] X. Zeng, A.-L. Ding, T. Liu, G.-C. Deng, X.-S. Zheng, W.-X. Cheng, J. Am. Ceram. Soc. 89 (2006) 728.
[7] C.L. Chen, H.H. Feng, Z. Zhang, A. Brazdeikis, Z.J. Huang, W.K. Chu, C.W. Chu, F.A. Miranda, F.W. Van Keuls, R.R. Romanofsky, Y. Liou, Appl. Phys. Lett. 75 (1999) 412.
[8] A.P. Ramirez, M.A. Subramanian, M. Gardel, G. Blumberg, D. Li, T. Vogt, S.M. Shapiro, Solid State Commun. 115 (2000) 217.
[9] M.A. Subramanian, D. Li, N. Duan, B.A. Reisner, A.W. Sleight, J. Solid State Chem. 151 (2000) 323.
[10] C.C. Homes, T. Vogt, S.M. Shapiro, S. Wakimoto, A.P. Ramirez, Science 293 (2001) 673.
[11] M.A. Subramanian, A.W. Sleight, Solid State Sci. 4 (2002) 347.
[12] D.C. Sinclair, T.B. Adams, F.D. Morrison, A.R. West, Appl. Phys. Lett. 80 (2002) 2153.
[13] T.B. Adams, D.C. Sinclair, A.R. West, Adv. Mater. 14 (2002) 1321.
[14] L. Fang, M. Shen, W. Cao, J. Appl. Phys. 95 (2004) 6483.
[15] S. Aygun, X. Tan, J.-P. Maria, D. Cann, J. Electroceram. 15 (2005) 203.
[16] B.A. Bender, M.-J. Pan, Mater. Sci. Eng., B, Solid-State Mater. Adv. Technol. 117 (2005) 339.
[17] J. Liu, C.-G. Duan, W.N. Mei, R.W. Smith, J.R. Hardy, J. Appl. Phys. 98 (2005) 93703.
[18] P. Lunkenheimer, R. Fichtl, S.G. Ebbinghaus, A. Loidl, Phys. Rev., B 70 (2004) 172102.
[19] Y. Lin, Y.B. Chen, T. Garret, S.W. Liu, C.L. Chen, L. Chen, R.P. Bontchev, A. Jacobson, J.C. Jiang, E.I. Meletis, J. Horwitz, H.-D. Wu, Appl. Phys. Lett. 81 (2002) 631.
[20] W. Si, E.M. Cruz, P.D. Johnson, P.W. Barnes, P. Woodward, A.P. Ramirez, Appl. Phys. Lett. 81 (2002) 2056.
[21] L. Chen, C.L. Chen, Y. Lin, Y.B. Chen, X.H. Chen, R.P. Bontchev, C.Y. Park, A.J. Jacobson, Appl. Phys. Lett. 82 (2003) 2317.
[22] Y.L. Zhao, G.W. Pan, Q.B. Ren, Y.G. Cao, L.X. Feng, Z.K. Jiao, Thin Solid Films 445 (2003) 7.
[23] W. Lu, L. Feng, G. Cao, Z. Jiao, J. Mater. Sci. 39 (2004) 3523.
[24] J. Liu, C.-G. Duan, W.-G. Yin, W.N. Mei, R.W. Smith, J.R. Hardy, Phys. Rev., B 70 (2004) 144106.